AGU PUBLICATIONS

JGR

Journal of Geophysical Research: Space Physics

RESEARCH ARTICLE
10.1002/2017JA024485

**Key Points:**
- Formation of local minimums in phase space density profiles of ultrarelativistic electrons coincides with EMIC wave occurrence
- New local minimums are accompanied by narrowing of normalized pitch angle distributions
- The local minimums are indicative of EMIC wave-induced loss in the heart of the outer belt

**Supporting Information:**
- Supporting Information S1

**Correspondence to:**
N. A. Aseev,
nikita.aseev@gfz-potsdam.de

**Citation:**
Aseev, N. A., Shprits, Y. Y., Drozdov, A. Y., Kellerman, A. C., Usanova, M. E., Wang, D., & Zhelavskaya, I. S. (2017). Signatures of ultrarelativistic electron loss in the heart of the outer radiation belt measured by Van Allen Probes. *Journal of Geophysical Research: Space Physics*, *122*. https://doi.org/10.1002/2017JA024485

Received 16 JUN 2017
Accepted 15 SEP 2017
Accepted article online 19 SEP 2017



# Signatures of Ultrarelativistic Electron Loss in the Heart of the Outer Radiation Belt Measured by Van Allen Probes

**N. A. Aseev[1,2], Y. Y. Shprits[1,2,3], A. Y. Drozdov[3], A. C. Kellerman[3], M. E. Usanova[4], D. Wang[1], and I. S. Zhelavskaya[1,2]**

[1]GFZ German Research Centre for Geosciences, Potsdam, Germany, [2]Institute of Physics and Astronomy, University of Potsdam, Potsdam, Germany, [3]Department of Earth, Planetary, and Space Sciences, University of California, Los Angeles, CA, USA, [4]Laboratory for Atmospheric and Space Physics, University of Colorado Boulder, Boulder, CO, USA

**Abstract** Up until recently, signatures of the ultrarelativistic electron loss driven by electromagnetic ion cyclotron (EMIC) waves in the Earth's outer radiation belt have been limited to direct or indirect measurements of electron precipitation or the narrowing of normalized pitch angle distributions in the heart of the belt. In this study, we demonstrate additional observational evidence of ultrarelativistic electron loss that can be driven by resonant interaction with EMIC waves. We analyzed the profiles derived from Van Allen Probe particle data as a function of time and three adiabatic invariants between 9 October and 29 November 2012. New local minimums in the profiles are accompanied by the narrowing of normalized pitch angle distributions and ground-based detection of EMIC waves. Such a correlation may be indicative of ultrarelativistic electron precipitation into the Earth's atmosphere caused by resonance with EMIC waves.

## 1. Introduction

Wave-particle interactions causing loss and acceleration of electrons in the Earth's radiation belts have been extensively studied since the beginning of the space era (Imhof et al., 1977; Millan & Thorne, 2007; Shprits, Elkington, et al., 2008; Shprits, Subbotin, et al., 2008; Thorne, 2010; Thorne & Kennel, 1971; Xiao et al., 2009, 2010). Recently, particular attention has been paid to the dynamics of very energetic ultrarelativistic electrons (energy above ~1–2 MeV) (e.g., Baker, Kanekal, Hoxie, Henderson, et al., 2013; Shprits et al., 2016; 2013, Xiao et al., 2015). However, major mechanisms controlling this population are still under debate. The purpose of this study is to provide additional observational evidence of ultrarelativistic electron loss due to local resonant interaction with electromagnetic ion cyclotron (EMIC) waves.

The launch of the Van Allen Probes, formerly known as Radiation Belt Storm Probes (RBSP), on 30 August 2012 has led to significant progress in understanding the dynamics of ultrarelativistic electron population. The Relativistic Electron-Proton Telescope (REPT) (Baker, Kanekal, Hoxie, Batiste, et al., 2013), which is a part of the Energetic Particle, Composition, and Thermal Plasma (ECT) Suite (Spence et al., 2013) on board the satellites, allows measuring the electron distribution of energies from ~2 to ~10 MeV and above and covers both inner and outer belt regions from 1.2 $R_E$ to 5.8 $R_E$. A few days after the launch, the Van Allen Probes detected the unusual three-zone radiation belt structure (Baker, Kanekal, Hoxie, Henderson, et al., 2013). The third belt (narrow "storage ring") (Baker, Kanekal, Hoxie, Henderson, et al., 2013) persisting for almost a month was formed by ultrarelativistic electrons at $L^*$ = ~3.25 after the flux dropout on approximately 3 September 2012. Shprits et al. (2013) analyzed this unique event, modeling the electron dynamics with the Versatile Electron Radiation Belt (VERB) code (Shprits et al. 2009; Subbotin & Shprits, 2009). They showed that EMIC wave-induced electron scattering is responsible for the formation of the third belt, and the expanded plasmasphere placed the belt in a different plasma environment, where electromagnetic waves weakly affect ultrarelativistic electrons, and the third belt remained for tens of days. Long-term modeling results obtained by Drozdov et al. (2015) using the VERB code showed that observed 3.6 MeV electron fluxes are significantly overestimated if EMIC waves are not included in the simulations. Further comparison of the simulation results with the observations of the 17 January 2013 storm (Shprits et al., 2016) confirmed that EMIC waves cause fast local loss of the ultrarelativistic electrons in the outer belt.

Previous theoretical studies suggested that EMIC waves can effectively scatter sub-MeV and MeV electrons (Horne & Thorne, 1998; Summers & Thorne, 2003; Thorne & Kennel, 1971; Ukhorskiy et al., 2010). Supporting the theoretical findings, a number of observational case studies used VLF transmitter and receiver systems, riometers, balloons, and polar satellites to measure ultrarelativistic electron precipitation associated with simultaneous EMIC wave detection by ground-based or satellite magnetometers (Blum et al., 2015; Clilverd et al., 2007, 2015, Miyoshi et al., 2008; Rodger et al., 2008, 2015). Using a recently developed algorithm for determination of precipitation events of sub-MeV and MeV electrons from Polar Orbiting Environmental Satellites (POES) and Meteorological Operational (METOP-2) satellite (Carson et al., 2013), Hendry et al. (2016) showed that 60% to 90% of precipitation events coincide with the waves detected on the ground. Yet the observational studies of electron precipitation into the atmosphere suggested that sub-MeV and MeV electrons can be scattered by EMIC waves, such studies consider only the electron population inside the loss cone, leaving aside the effects of the waves on the pitch angle distribution of particles in the heart of the belt.

Usanova et al. (2014) investigated the correlation between ground-based EMIC wave observations from the Canadian Array for Real-time Investigations of Magnetic Activity (CARISMA) (Mann et al., 2008) and the variability of the ultrarelativistic outer belt measured in situ by the Van Allen Probes. They found the correlation between the observations of EMIC waves and narrowing of the normalized pitch angle distributions, which is a clear tell-tale signature of EMIC wave-induced precipitation.

Another mechanism of electron loss affecting all populations of radiation belt particles is the loss into the interplanetary medium driven by outward radial diffusion (Ohtani et al., 2009; Shprits et al., 2006; Turner et al., 2012). This mechanism is most effective during compression of the magnetosphere when particles previously trapped in the Earth's magnetic field at high radial distances find themselves drifting along the open trajectories that cross the magnetopause. These particles become lost into the interplanetary medium on time scales of the drift period, creating sharp negative gradients near the outer boundary of the outer belt. The sharp gradients, in turn, result in fast particle transport away from Earth due to enhanced outward radial diffusion driven by drift resonance of particles with ultralow frequency (ULF) waves. The loss into the interplanetary medium should be carefully separated from the precipitation into the atmosphere if any loss mechanism in the belts is investigated.

In this study, we present additional evidence for the ultrarelativistic electron loss in the heart of the outer belt that can be driven by resonant interaction with EMIC waves and complement the signatures of EMIC wave effects found by Usanova et al. (2014) for the time period from 9 October to 29 November 2012. We analyze phase space densities (PSD), derived from Van Allen Probe observations as a function of time and three adiabatic invariants $\mu$, $K$, and $L^*$ (Roederer, 2012; Schulz & Lanzerotti, 1974), to distinguish reversible (adiabatic) changes resulting from slow expansion and compression of the magnetic field from nonreversible (nonadiabatic) changes leading to particle loss or acceleration. The mechanisms causing nonreversible changes can be further differentiated if the PSD is considered as a function of $L^*$ and time for constant $\mu$ and $K$ (Green & Kivelson, 2004; Reeves et al., 2013; Selesnick & Blake, 2000). In particular, local minimums in relativistic and ultrarelativistic electron PSD profiles are a distinctive feature of fast local loss, which can be driven by EMIC waves (Shprits et al., 2017). To provide observational evidence that EMIC waves scatter ultrarelativistic electrons into the Earth's atmosphere, we analyze such local minimums, narrowing of pitch angle distributions and the occurrence of EMIC waves on the ground.

## 2. Van Allen Probe Flux Measurements From 9 October to 29 November 2012

The interval of enhanced ultrarelativistic electron flux in the outer belt between 9 October and 29 November 2012 was teemed with multiple events of enhanced EMIC wave activity observed on the ground (Usanova et al., 2014) and gave us a good opportunity to gain insight into the processes driving the electron loss. Figure 1 illustrates the dynamics of differential ultrarelativistic electron fluxes from 9 October to 29 November. Note that the fluxes were averaged over the solid angle subtended by a whole sphere. Figure 1a shows the evolution of *Dst* and *Kp* indices, and Figures 1b–1d present the fluxes measured by the REPT instrument on board the Van Allen Probes. Figure 1e, adopted from Usanova et al. (2014), demonstrates the occurrence of EMIC waves on the ground measured by CARISMA stations at $L = 4–4.5$. The red circles in Figure 1e denote the days when EMIC waves were observed, while blue circles indicate the days when no EMIC wave activity was detected.

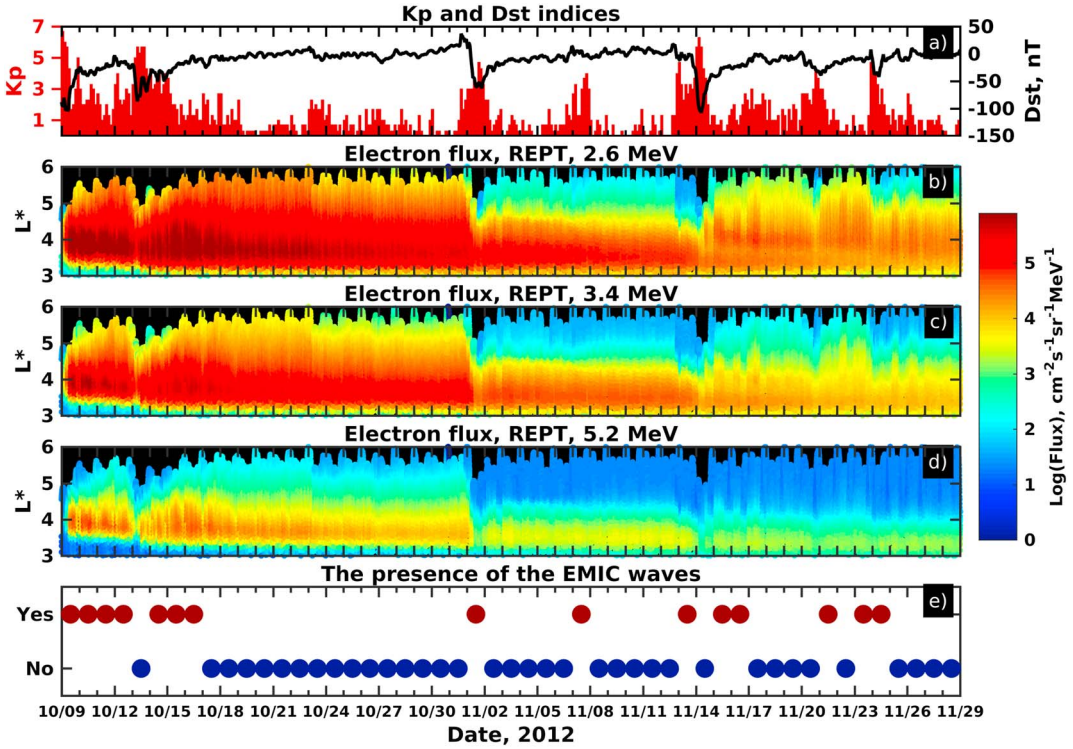


**Figure 1.** (a) *Kp* and *Dst* indices between 9 October and 29 November 2012, provided by OMNIWeb. (b–d) Differential electron fluxes measured by REPT on board Van Allen Probes in 2.6, 3.4, and 5.2 MeV energy channels as a function of time and $L^*$ computed using the TS07D magnetic field model (Tsyganenko & Sitnov, 2007). (e) The presence of EMIC waves measured by CARISMA stations at $L = 4–4.5$.

The prominent storm time flux dropouts are observed on 13 October, 1 November, and 13–14 November. The dropouts are accompanied by enhanced EMIC wave activity and minimums in the *Dst* index, which indicates that EMIC wave-induced scattering, adiabatic changes associated with the changes in the magnetic field configuration, magnetopause shadowing, and the loss into the interplanetary medium driven by outward radial diffusion can be responsible for such flux variations. Interestingly, EMIC waves are also observed not only during dropouts but also during the enhancement of the belt (e.g., 14–16 October) and intervals when the flux remains almost unchanged (e.g., 7 November 2012). It is therefore necessary to distinguish between competing loss and acceleration processes while performing analysis of EMIC wave effects on ultrarelativistic electrons in the belt.

## 3. Data and Methods

In order to extract signatures of EMIC wave-driven ultrarelativistic electron loss from in situ Van Allen Probe measurements, we applied the method proposed by Shprits et al. (2017). The method relies on the fact that interacting locally with electrons, EMIC waves produce pronounced local minimums in PSD profiles for constant first and second adiabatic invariants. Unless smoothed out by radial diffusion or local acceleration, the minimums can persist for hours and days, and they can be derived from the Van Allen Probe ECT suite observations.

We used 5 min averaged Magnetic Electron Ion Spectrometer (MagEIS) (Blake et al., 2013) and REPT data to calculate electron PSD as a function of adiabatic invariants. The first adiabatic invariant $\mu$ has been calculated using local magnetic field observations measured by the Electric and Magnetic Field Instrument Suite and Integrated Science (Kletzing et al., 2013) on the satellites. To determine the invariants $K$ and $L^*$ corresponding to the local pitch angles and position of satellites, we utilized the TS07D magnetic field model (Tsyganenko & Sitnov, 2007), which is implemented in the International Radiation Belt Environment Modeling (IRBEM) library (Boscher et al., 2012). We calculated PSD for $K = 0.1G^{1/2}R_E$, since this value of the second invariant roughly corresponds to 51°–55° pitch angles in the heart of the outer belt, and EMIC waves can efficiently resonate

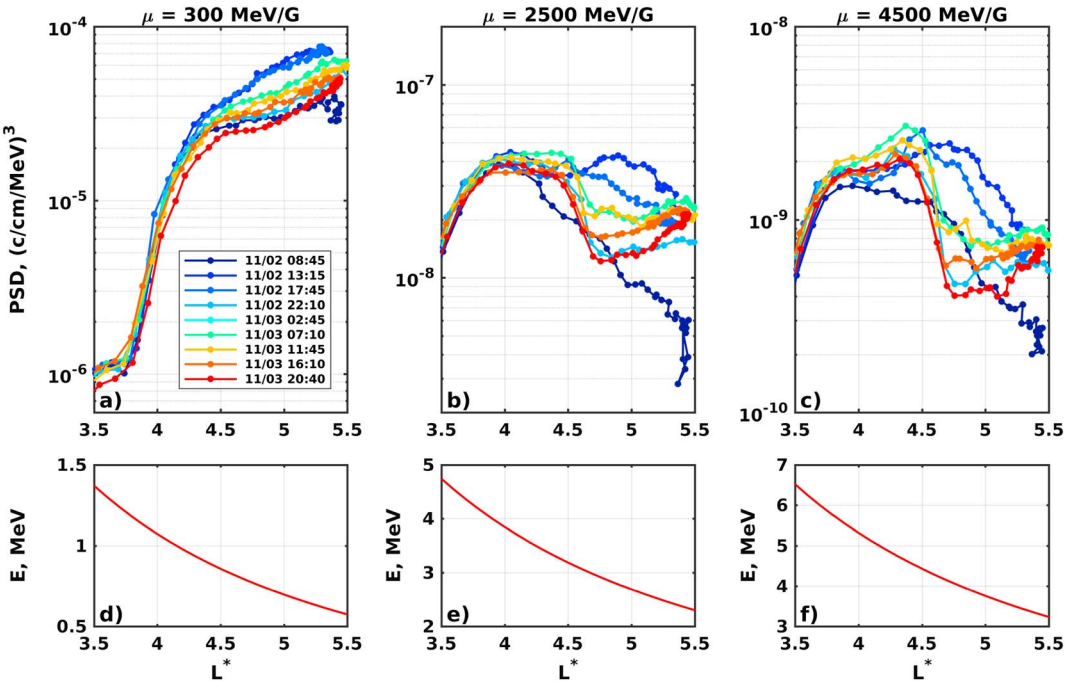


**Figure 2.** (a–c) Evolution of PSD profiles derived from RBSP-A flux measurements as a function of $L^*$ for $K = 0.1G^{1/2}\ R_E$ and $\mu$ = 300, 2,500, and 4,500 MeV/G on 2–3 November 2012 using the TS07D magnetic field model. The colors represent the end times of successive inbound and outbound satellite passes. (d–f) Energies corresponding to the chosen $\mu$ and $K$ calculated in the dipole field approximation.

with the ultrarelativistic electrons of such pitch angles (Summers & Thorne, 2003). We used bilinear cubic interpolation to calculate PSD for particular values of $\mu$ and $K$ for constant $L^*$.

## 4. Signatures of EMIC Wave-Driven Ultrarelativistic Electron Loss

Figure 2 illustrates the formation of local minimums on 2–3 November after the dropout of electron fluxes on 1 November (see Figures 1b–1d). Figures 2a–2c show the evolution of relativistic ($\mu$ =300 MeV/G) and ultrarelativistic ($\mu$ = 2,500 and 4,500 MeV/G) PSD profiles. Figures 2d–2f depict energies corresponding to the chosen adiabatic invariants in the dipole field approximation. Predropout ultrarelativistic profiles, derived from RBSP-A measurements at around 08:45, 2 November, have wide pronounced peaks at $L^* = 4$ and negative gradients above $L^* = \sim 4.3$ (see dark blue lines in Figures 2b and 2c). The next two passes of RBSP-A show an enhancement of both relativistic and ultrarelativistic electron PSD at higher L shells. The formation of local minimums can be noticed at the following satellite pass at $L^* = \sim 4.7$ around 22:10. The passes at ~07:10 and ~11:45 on 3 November show enhancement of ultrarelativistic electron PSD above $L^* = \sim 4.5$ without noticeable changes in the depth and width of the minimums. The subsequent passes demonstrate fast deepening of local minimums at $L^* = 4.7$, while profiles at $L^* = 5.5$ do not show significant variations. Relativistic electron profiles, presented in Figure 2a, preserve monotonic behavior for the considered interval, showing only a slow gradual decrease.

To take into account uncertainties associated with calculations of $K$ and $L^*$ that globally depend on magnetic field configuration, we analyzed PSD profiles computed using T89 (Tsyganenko, 1989), T96 (Tsyganenko, 1995), T01S (Tsyganenko, 2002), and T04S (Tsyganenko & Sitnov, 2005) magnetic field models. Supporting information Figures S1–S4 correspond to the profiles derived on the basis of these models. The figures show that the local minimums in ultrarelativistic electron PSD profiles are observed independently of any known advanced magnetic field model, while relativistic electron profiles demonstrate a monotonic decrease with $L^*$.

The simultaneous formation of local minimums in ultrarelativistic electron PSD profiles at $L^* = 4.7$, the decrease between $L^* = 4.5$ and 5, and slight changes at $L^* = 5.5$ imply a fast local loss process operating in a narrow region of L shells. The observed minimums could not be produced by magnetopause shadowing

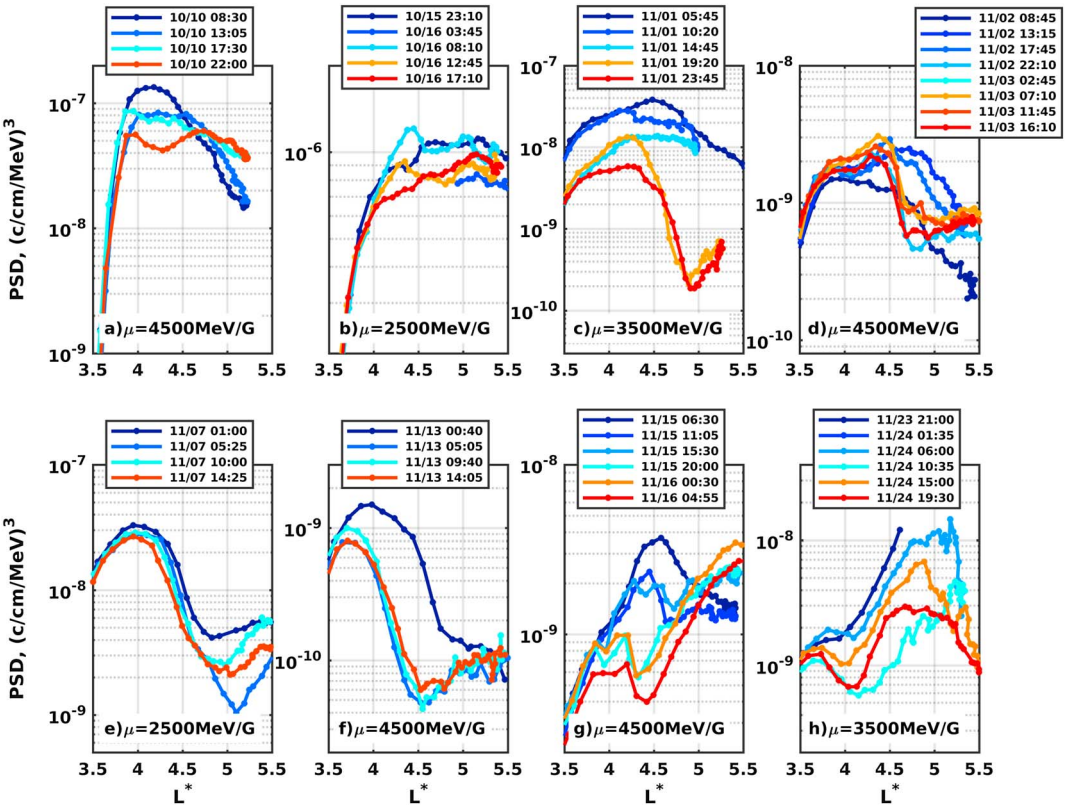


**Figure 3.** (a–h) Evolution of PSD profiles during periods when the most pronounced minimums were detected. The profiles are derived from RBSP-A flux measurements as a function of $L^*$ for $K = 0.1\ G^{1/2}\ R_E$ and constant $\mu$ computed using the TS07D magnetic field model. Colors represent the end times of successive inbound and outbound satellite passes.

or by the local interaction with hiss or chorus waves, which is effective on the much longer time scales than the Van Allen Probe orbital period and characterized by a very weak dependence on radial distance (Orlova & Shprits, 2014; Orlova et al., 2014; Shprits et al., 2017). EMIC waves, resonating with ultrarelativistic electrons, can locally scatter electrons into the loss cone and form the minimums, as presented in Figures 2b and 2c. The absence of such minimums in the profiles of less energetic electrons (Figure 2a) is additional evidence of an EMIC wave-driven nature of loss, since less energetic electrons do not interact with EMIC waves according to the concept of minimum resonant energy (e.g., Summers & Thorne, 2003).

We analyzed PSD profiles for $\mu$ = 2,500, 3,500, and 4,500 MeV/G from 9 October to 29 November 2016 and found eight events when noticeable local minimums were formed for at least one value of $\mu$ in the chosen range. Figures 3a–3h show the profiles for the values of the first invariant $\mu$ corresponding to the most pronounced minimums observed. The minimums differ in their position, depth, and width. The minimums are located between $L^*$ = 4 and 5, and the width varies from ~0.3 to ~1 (in L shell units). The minimums appear simultaneously with the prominent dropouts (Figures 3c, 3f, and 3h) of PSD, or when no large variations of PSD detected (Figures 3a, 3b, 3d, 3e, and 3g). To diminish uncertainties associated with the magnetic field model, we also analyzed PSD profiles calculated using the T04S magnetic field model for identified events. Supporting information Figure S5 shows that the change in the magnetic field model mostly does not affect local minimums, though their shape can be slightly different.

Figure 4 summarizes the signatures of EMIC wave effects on ultrarelativistic electrons in the outer belt for the studied period. Figure 4a illustrates the occurrence of EMIC waves on the ground and is similar to Figure 1e. Figure 4b shows the presence of new pronounced local minimums in $\mu$ = 2,500, 3,500, or 4,500 MeV/G profiles. Red markers ("Yes") indicate days when the new local minimum was formed for at least one value in the chosen range, and blue markers ("No") represent days without local minimums. Figures 4c–4e illustrate the pitch angle distributions of differential fluxes normalized by the equatorial flux at $L^*$ = 4.5 in the energy channels 2.6, 3.4, and 5.2 MeV.

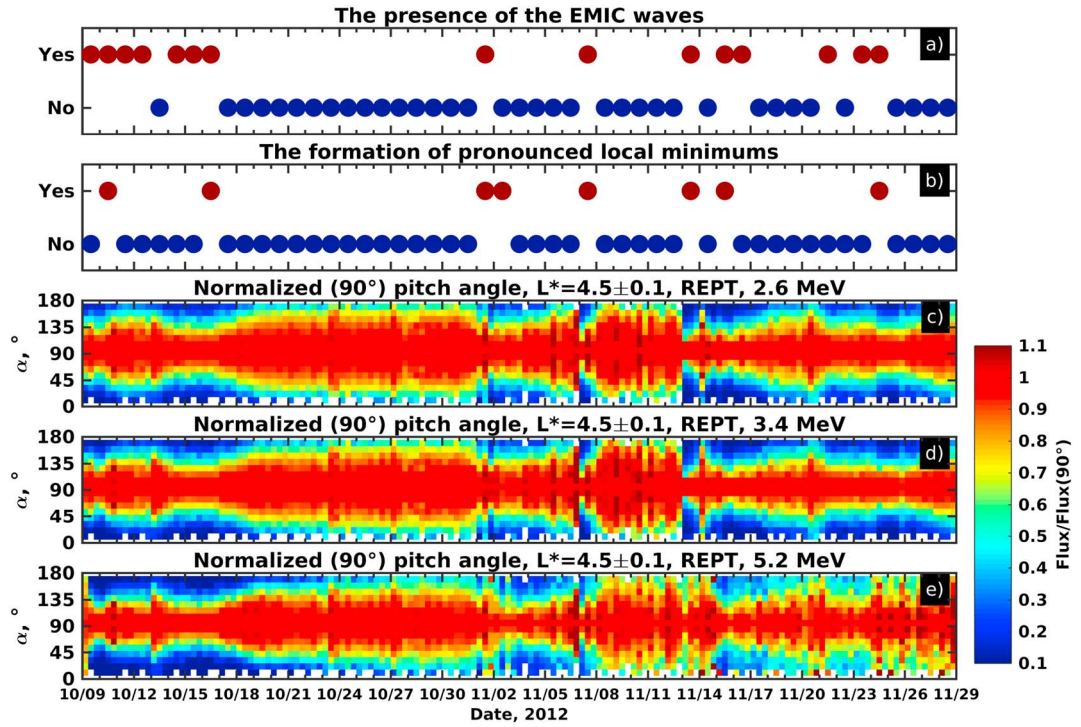


**Figure 4.** (a) The presence of EMIC waves measured by CARISMA stations between 9 October and 29 November 2012. (b) The formation of new local minimums in PSD profiles for the same time period. (c–e) The pitch angle distributions of directional differential fluxes normalized by the equatorial flux as a function of time and pitch angles measured by Van Allen Probes in 2.6, 3.4, and 5.2 MeV energy channels at $L^* = 4.5 \pm 0.1$.

New local minimums are formed during intervals of high EMIC wave activity, demonstrating strong correlation with the detection of EMIC waves on the ground (compare red dots in Figures 4a and 4b). The formation of local minimums also coincides with the narrowing of pitch angle distributions, produced by the resonant interaction with EMIC waves (Usanova et al., 2014). The simultaneous formation of local minimums, narrowing of the distributions, and EMIC wave detection on the ground is the observational evidence that EMIC waves not only change the shape of the normalized pitch angle distribution but may also result in particle loss.

## 5. Discussion

In this study, we analyzed 51 days of data measured by REPT on board the Van Allen Probes and found eight events of the formation of minimums in ultrarelativistic electron PSD profiles. The events were accompanied by the narrowing of normalized pitch angle distributions and EMIC wave detection on the ground (see Figure 4). Such correlation shows from the statistical point of view that the new local minimums have an EMIC wave-driven nature, as was found from the physical principles by Shprits et al. (2017). Complementing the findings of Usanova et al. (2014), which demonstrate that the narrowing of the pitch angle distributions coincides with EMIC wave measurements, the formation of new local minimums may indicate EMIC wave-induced scattering of ultrarelativistic electrons.

The new local minimums not only provide evidence of ultrarelativistic electron loss but can also help identify EMIC wave occurrence in space. Since the minimums are the response of the electrons to the wave activity, they are the explicit manifestation of EMIC waves even if wave measurements are not available or spacecraft is not in the region of the waves. Therefore, the new minimums can be used to support direct observations of the waves or to reveal EMIC waves that cannot be observed on the ground or in situ. Seven of eight local minimums found between 9 October and 29 November 2012 serve as additional evidence of EMIC wave presence, while only one local minimum, which appeared on 2 November after the previous minimum on 1 November vanished, was not accompanied by EMIC waves and can be considered a potential indirect signature of the waves (see Figure 4).

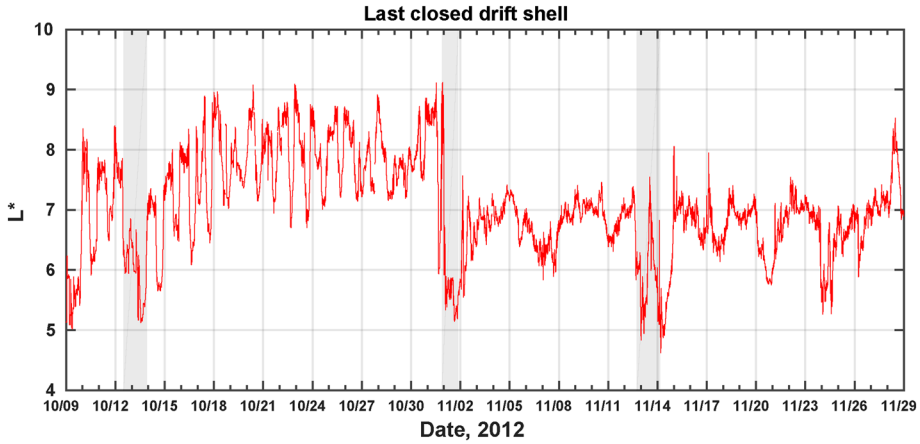


**Figure 5.** The last closed drift shell computed for equatorially mirroring particles using the TS07D magnetic field model. The gray shadowed regions correspond to significant storm time dropouts of ultrarelativitic electron fluxes at $L^* = 5$.

The duration of EMIC waves can be estimated from electron flux observations (converted to PSD) in case of deepening minimums as was discussed by Shprits et al. (2017). The deepening minimum in ultrarelativistic electron PSD profiles indicates that local loss induced by EMIC waves dominates over the acceleration process driven by radial diffusion that tends to smooth out the minimum. In this case, EMIC waves are present in the region of the deepening minimum at least as long as the deepening minimum is observed. However, if the minimum does not change its depth or the depth decreases, it is hard to distinguish EMIC wave effects on radiation belt electrons from the radial diffusion influence using only flux observations, and more detailed analysis involving EMIC wave parameters and radial diffusion rates is required. For this reason, we do not consider the question of EMIC wave duration in the current study and concentrate only on EMIC wave presence, which can be evident from the event of new local minimum formation.

The analysis of minimums can be complicated by different loss and acceleration processes that occur simultaneously with EMIC waves. For instance, Figure 3b shows the acceleration of particles after the minimum is formed at ~12:45 on 16 October. In this case, the acceleration over the wide $L^*$ range may accompany the loss of ultrarelativistic particles at $L^* = \sim 4.6$. Electron acceleration may render the minimums more shallow that is harder to detect visually or by using an automated algorithm.

For some events, EMIC waves were observed at times when local minimums are not seen in the data. That can be explained by the action of radial diffusion smoothing out the minimums, competition with local acceleration, or nonoptimal spectral properties of the waves for the efficient electron scattering. For instance, if the local minimum is formed at high L shells, it can be suddenly destroyed by magnetopause shadowing, as was detected on 12 November (see supporting information Figure S6). Acceleration due to inward radial diffusion or local interaction with nightside chorus waves can lead to the increase in PSD and smoothing out the minimums (see supporting information Figure S7 illustrating the disappearance of the minimums on 2 November). If competing processes significantly distort the minimums on time scales less than half of the Van Allen Probe period, the local minimums can be hardly observed, and therefore, their formation is detected more rarely than EMIC waves.

The local minimums and narrowing of pitch angle distributions are observed during the intervals of prominent storm time flux dropouts, indicating that EMIC waves can contribute to the noticeable flux decrease. It is necessary, however, to estimate the relative importance of EMIC wave-induced loss in the outer belt and the loss into the interplanetary medium driven by outward radial diffusion. Figure 5 shows the last closed drift shell calculated for equatorially mirroring electrons using the TS07D magnetic field model. To calculate the last closed drift shell, we find the farthest from the Earth magnetic field line that has only one local minimum at the noon magnetic longitude and calculate $L^*$ corresponding to a given $K$ value. This approach is implemented because of the limitations of IRBEM model computational framework to deal with double minimum field lines and provides an approximation of the last closed drift shell, which likely is at slightly higher L shells. A gray background color in Figure 5 marks the periods when the significant storm time dropouts of

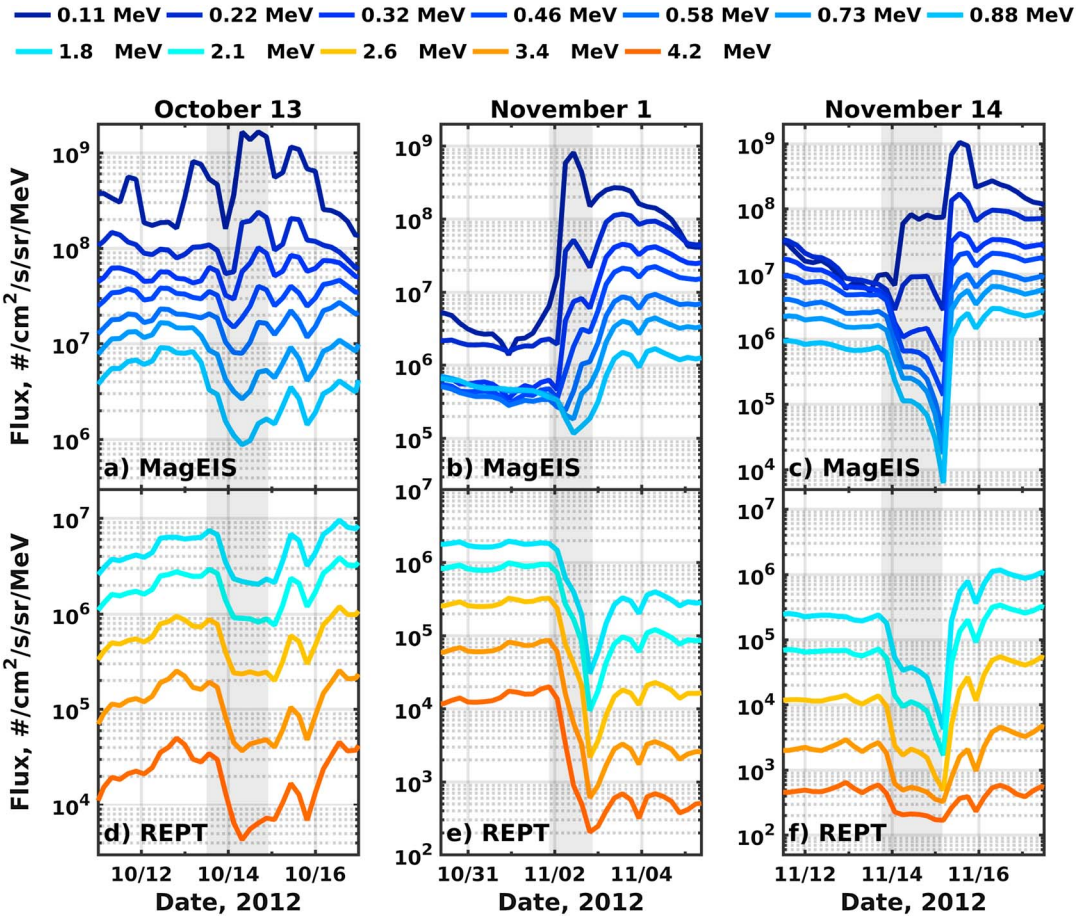


**Figure 6.** Evolution of electron fluxes at $L^* = 5 \pm 0.25$ measured by MagEIS and REPT instruments on board the RBSP-A during the most significant storm time dropouts that occurred on (a, d) 13 October, (b, e) 1 November, and (c, f) 13–14 November. The fluxes are averaged over the satellite orbital period. The gray shaded regions correspond to significant storm time dropouts of ultrarelativistic electron fluxes.

the ultrarelativistic electron fluxes were observed at $L^* = 5$. As can be clearly seen from the figure, all storm time events were accompanied by the sharp decrease of the last closed drift shell, which may indicate the enhanced electron loss into the interplanetary medium.

Figure 6 illustrates electron fluxes measured by the RBSP-A at $L^* = 5$ and averaged over the satellite orbital period for the storms that occurred on 13 October, 1 November, and 13–14 November. The storms on 13 October and 13–14 November are characterized by a simultaneous dropout in electron fluxes from ~100–200 keV to several MeV energies (gray shaded regions in Figures 6a and 6d and Figures 6c and 6f), which can be indicative of the radiation belt variations associated with changes in magnetic field configuration. The event on 1 November, however, shows a significant decrease of multi-MeV electron fluxes and a simultaneous increase in ~100–800 keV fluxes (see Figures 6b and 6e). The flux enhancement can be driven by electron injections from the plasma sheet into the radiation belt region, concealing any possible effects of magnetopause shadowing on such electron population. Modeling studies (e.g., Drozdov et al., 2015; Kersten et al., 2014; Shprits et al., 2016) are required for further understanding of the balance between EMIC wave loss, loss into the interplanetary medium, and the electron source population injected at the nightside.

We emphasize the existence of essential coherence between EMIC wave observations and new local minimums in PSD profiles of ultrarelativistic electrons. Further studies are required for detailed understanding of correlations between the waves and the minimums, conditions under which the minimums are formed, and dependence of local minimum parameters on EMIC wave properties.

**Acknowledgments**
The authors used geomagnetic indices provided by OMNIWeb (http://omniweb.gsfc.nasa.gov/form/dx1.html) and are grateful to the RBSP-ECT team for the provision of Van Allen Probes observations (http://rbsp-ect.lanl.gov/). This research was supported by the Helmholtz-Gemeinschaft (HGF) [10.13039/501100001656], NSFGEM AGS-1203747, NASA grant NNX12AE34G, NASA grant NNX16AF91G, and project PROGRESS funded by EC | Horizon 2020 Framework Programme (H2020) [10.13039/100010661] (637302)). The authors are grateful to Sharon Uy for the help with editing the paper. The authors thank anonymous reviewers for their insightful comments that helped to improve the manuscript. This work used computational and storage services associated with the Hoffman2 Shared Cluster provided by UCLA Institute for Digital Research and Education's Research Technology Group. The research has been partially funded by Deutsche Forschungsgemeinschaft (DFG) through grant CRC 1294 "Data Assimilation," Project B06 Novel methods for the 3-D reconstruction of the dynamic evolution of the Van Allen belts using multiple satellite measurements. The authors thank the developers of the IRBEM library, which was adapted for use in the current study. The authors thank Geoffrey Reeves for his help on the Van Allen Probe data quality.

## References

Baker, D. N., Kanekal, S. G., Hoxie, V. C., Batiste, S., Bolton, M., Li, X., … Friedel, R. (2013). The Relativistic Electron-Proton Telescope (REPT) instrument on board the Radiation Belt Storm Probes (RBSP) spacecraft: Characterization of Earth's radiation belt high-energy particle populations. *Space Science Reviews*, *179*(1–4), 337–381. https://doi.org/10.1007/s11214-012-9950-9

Baker, D. N., Kanekal, S. G., Hoxie, V. C., Henderson, M. G., Li, X., Spence, H. E., … Claudepierre, S. G. (2013). A long-lived relativistic electron storage ring embedded in Earth's outer Van Allen belt. *Science*, *340*, 6129. https://doi.org/10.1126/science.1233518

Blake, J. B., Carranza, P. A., Claudepierre, S. G., Clemmons, J. H., Crain, W. R., Dotan, Y., … Zakrzewski, M. P. (2013). The Magnetic Electron Ion Spectrometer (MAGEIS) instruments aboard the Radiation Belt Storm Probes (RBSP) spacecraft. *Space Science Reviews*, *179*(1–4), 383–421. https://doi.org/10.1007/s11214-013-9991-8

Blum, L. W., Halford, A., Millan, R., Bonnell, J. W., Goldstein, J., Usanova, M., … Li, X. (2015). Observations of coincident EMIC wave activity and duskside energetic electron precipitation on 18–19 January 2013. *Geophysical Research Letters*, *42*, 5727–5735. https://doi.org/10.1002/2015GL065245

Boscher, D., Bourdarie, S., O'Brien, P., & Guild, T. (2012). Irbem-lib librarym. Retrieved from http://irbem.sourceforge.net

Carson, B. R., Rodger, C. J., & Clilverd, M. A. (2013). POES satellite observations of EMIC-wave driven relativistic electron precipitation during 1998–2010. *Journal of Geophysical Research: Space Physics*, *118*, 232–243. https://doi.org/10.1029/2012JA017998

Clilverd, M. A., Rodger, C. J., Millan, R. M., Sample, J. G., Kokorowski, M., McCarthy, M. P., … Spanswick, E. (2007). Energetic particle precipitation into the middle atmosphere triggered by a coronal mass ejection. *Journal of Geophysical Research*, *112*, A12206. https://doi.org/10.1029/2007JA012395

Clilverd, M. A., Duthie, R., Hardman, R., Hendry, A. T., Rodger, C. J., Raita, T., … Milling, D. K. (2015). Electron precipitation from EMIC waves: A case study from 31 May 2013. *Journal of Geophysical Research: Space Physics*, *120*, 3618–3631. https://doi.org/10.1002/2015JA021090

Drozdov, A. Y., Shprits, Y. Y., Orlova, K. G., Kellerman, A. C., Subbotin, D. A., Baker, D. N., … Reeves, G. D. (2015). Energetic, relativistic, and ultrarelativistic electrons: Comparison of long-term VERB code simulations with Van Allen Probes measurements. *Journal of Geophysical Research: Space Physics*, *120*, 3574–3587. https://doi.org/10.1002/2014JA020637

Green, J. C., & Kivelson, M. G. (2004). Relativistic electrons in the outer radiation belt: Differentiating between acceleration mechanisms. *Journal of Geophysical Research*, *109*, A03213. https://doi.org/10.1029/2003JA010153

Hendry, A. T., Rodger, C. J., Clilverd, M. A., Engebretson, M. J., Mann, I. R., Lessard, M. R., … Milling, D. K. (2016). Confirmation of EMIC wave-driven relativistic electron precipitation. *Journal of Geophysical Research: Space Physics*, *121*, 5366–5383. https://doi.org/10.1002/2015JA022224

Horne, R. B., & Thorne, R. M. (1998). Potential waves for relativistic electron scattering and stochastic acceleration during magnetic storms. *Geophysical Research Letters*, *25*(15), 3011–3014. https://doi.org/10.1029/98GL01002

Imhof, W. L., Reagan, J. B., & Gaines, E. E. (1977). Fine-scale spatial structure in the pitch angle distributions of energetic particles near the midnight trapping boundary. *Journal of Geophysical Research*, *82*(32), 5215–5221. https://doi.org/10.1029/JA082i032p05215

Kersten, T., Horne, R. B., Glauert, S. A., Meredith, N. P., Fraser, B. J., & Grew, R. S. (2014). Electron losses from the radiation belts caused by EMIC waves. *Journal of Geophysical Research: Space Physics*, *119*, 8820–8837. https://doi.org/10.1002/2014JA020366

Kletzing, C. A., Kurth, W. S., Acuna, M., MacDowall, R. J., Torbert, R. B., Averkamp, T., … Tyler, J. (2013). The Electric and Magnetic Field Instrument Suite and Integrated Science (EMFISIS) on RBSP. *Space Science Reviews*, *179*(1–4), 127–181. https://doi.org/10.1007/s11214-013-9993-6

Mann, I. R., Milling, D. K., Rae, I. J., Ozeke, L. G., Kale, A., Kale, Z. C., … Singer, H. J. (2008). The upgraded CARISMA magnetometer array in the THEMIS era. *Space Science Reviews*, *141*(1–4), 413–451. https://doi.org/10.1007/s11214-008-9457-6

Millan, R. M., & Thorne, R. M. (2007). Review of radiation belt relativistic electron losses. *Journal of Atmospheric and Solar-Terrestrial Physics*, *69*, 362–377. https://doi.org/10.1016/j.jastp.2006.06.019

Miyoshi, Y., Sakaguchi, K., Shiokawa, K., Evans, D., Albert, J., Connors, M., & Jordanova, V. (2008). Precipitation of radiation belt electrons by EMIC waves, observed from ground and space. *Geophysical Research Letters*, *35*(23), L23101. https://doi.org/10.1029/2008GL035727

Ohtani, S., Miyoshi, Y., Singer, H. J., & Weygand, J. M. (2009). On the loss of relativistic electrons at geosynchronous altitude: Its dependence on magnetic configurations and external conditions. *Journal of Geophysical Research*, *114*, A01202. https://doi.org/10.1029/2008JA013391

Orlova, K., & Shprits, Y. (2014). Model of lifetimes of the outer radiation belt electrons in a realistic magnetic field using realistic chorus wave parameters. *Journal of Geophysical Research: Space Physics*, *119*, 770–780. https://doi.org/10.1002/2013JA019596

Orlova, K., Spasojevic, M., & Shprits, Y. (2014). Activity-dependent global model of electron loss inside the plasmasphere. *Geophysical Research Letters*, *41*, 3744–3751. https://doi.org/10.1002/2014GL060100

Reeves, G. D., Spence, H. E., Henderson, M. G., Morley, S. K., Friedel, R. H. W., Funsten, H. O., … Niehof, J. T. (2013). Electron acceleration in the heart of the Van Allen radiation belts. *Science*, *341*, 991–994. https://doi.org/10.1126/science.1237743

Rodger, C. J., Raita, T., Clilverd, M. A., Seppälä, A., Dietrich, S., Thomson, N. R., & Ulich, T. (2008). Observations of relativistic electron precipitation from the radiation belts driven by EMIC waves. *Geophysical Research Letters*, *35*, L16106. https://doi.org/10.1029/2008GL034804

Rodger, C. J., Hendry, A. T., Clilverd, M. A., Kletzing, C. A., Brundell, J. B., & Reeves, G. D. (2015). High-resolution in situ observations of electron precipitation-causing EMIC waves. *Geophysical Research Letters*, *42*, 9633–9641. https://doi.org/10.1002/2015GL066581

Roederer, J. G. (2012). *Dynamics of Geomagnetically Trapped Radiation* (Vol. 2). New York: Springer Science & Business Media.

Schulz, M., & Lanzerotti, L. J. (1974). *Particle diffusion in the radiation belts*, Physics and Chemistry in Space (Vol. 7). Berlin, Heidelberg: Springer Berlin Heidelberg. https://doi.org/10.1007/978-3-642-65675-0

Selesnick, R. S., & Blake, J. B. (2000). On the source location of radiation belt relativistic electrons. *Journal of Geophysical Research*, *105*(A2), 2607–2624. https://doi.org/10.1029/1999JA900445

Shprits, Y. Y., Subbotin, D., & Ni, B. (2009). Evolution of electron fluxes in the outer radiation belt computed with the VERB code. *Journal of Geophysical Research*, *114*, A11209. https://doi.org/10.1029/2008JA013784

Shprits, Y. Y., Elkington, S. R., Meredith, N. P., & Subbotin, D. A. (2008). Review of modeling of losses and sources of relativistic electrons in the outer radiation belt I: Radial transport. *Journal of Atmospheric and Solar-Terrestrial Physics*, *70*(14), 1679–1693. https://doi.org/10.1016/j.jastp.2008.06.008

Shprits, Y. Y., Subbotin, D. A., Meredith, N. P., & Elkington, S. R. (2008). Review of modeling of losses and sources of relativistic electrons in the outer radiation belt II: Local acceleration and loss. *Journal of Atmospheric and Solar-Terrestrial Physics*, *70*(14), 1694–1713. https://doi.org/10.1016/j.jastp.2008.06.014

Shprits, Y. Y., Thorne, R. M., Friedel, R., Reeves, G. D., Fennell, J., Baker, D. N., & Kanekal, S. G. (2006). Outward radial diffusion driven by losses at magnetopause. *Journal of Geophysical Research*, *111*, A11214. https://doi.org/10.1029/2006JA011657

Shprits, Y. Y., Kellerman, A., Aseev, N., Drozdov, A. Y., & Michaelis, I. (2017). Multi-MeV electron loss in the heart of the radiation belts. *Geophysical Research Letters*, *44*, 1204–1209. https://doi.org/10.1002/2016GL072258

Shprits, Y. Y., Subbotin, D., Drozdov, A., Usanova, M. E., Kellerman, A., Orlova, K., … Kim, K.-C. (2013). Unusual stable trapping of the ultrarelativistic electrons in the Van Allen radiation belts. *Nature Physics*, *9*(11), 699–703. https://doi.org/10.1038/nphys2760

Shprits, Y. Y., Drozdov, A. Y., Spasojevic, M., Kellerman, A. C., Usanova, M. E., Engebretson, M. J., … Aseev, N. A. (2016). Wave-induced loss of ultra-relativistic electrons in the Van Allen radiation belts. *Nature Communications*, *7*(12), 883. https://doi.org/10.1038/ncomms12883

Spence, H. E., Reeves, G. D., Baker, D. N., Blake, J. B., Bolton, M., Bourdarie, S., … Thorne, R. M. (2013). Science goals and overview of the Radiation Belt Storm Probes (RBSP) Energetic Particle, Composition, and Thermal Plasma (ECT) suite on NASA's Van Allen Probes mission. *The Van Allen Probes Mission*, *179*(1–4), 311–336. https://doi.org/10.1007/978-1-4899-7433-4-10

Subbotin, D. A., & Shprits, Y. Y. (2009). Three-dimensional modeling of the radiation belts using the Versatile Electron Radiation Belt (VERB) code. *Space Weather*, *7*, S10001. https://doi.org/10.1029/2008SW000452

Summers, D., & Thorne, R. M. (2003). Relativistic electron pitch-angle scattering by electromagnetic ion cyclotron waves during geomagnetic storms. *Journal of Geophysical Research*, *108*(A4), 1143. https://doi.org/10.1029/2002JA009489

Thorne, R. M. (2010). Radiation belt dynamics: The importance of wave-particle interactions. *Geophysical Research Letters*, *37*, L22107. https://doi.org/10.1029/2010GL044990

Thorne, R. M., & Kennel, C. F. (1971). Relativistic electron precipitation during magnetic storm main phase. *Journal of Geophysical Research*, *76*(19), 4446–4453. https://doi.org/10.1029/JA076i019p04446

Tsyganenko, N. A. (1989). A magnetospheric magnetic field model with a warped tail current sheet. *Planetary and Space Science*, *37*(1), 5–20. https://doi.org/10.1016/0032-0633(89)90066-4

Tsyganenko, N. A. (1995). Modeling the Earth's magnetospheric magnetic field confined within a realistic magnetopause. *Journal of Geophysical Research*, *100*(A4), 5599. https://doi.org/10.1029/94JA03193

Tsyganenko, N. A. (2002). A model of the near magnetosphere with a dawn-dusk asymmetry 1. Mathematical structure. *Journal of Geophysical Research*, *107*(A8), SMP 12–1–SMP 12-15. https://doi.org/10.1029/2001JA000219

Tsyganenko, N. A., & Sitnov, M. I. (2005). Modeling the dynamics of the inner magnetosphere during strong geomagnetic storms. *Journal of Geophysical Research*, *110*, A03208. https://doi.org/10.1029/2004JA010798

Tsyganenko, N. A., & Sitnov, M. I. (2007). Magnetospheric configurations from a high-resolution data-based magnetic field model. *Journal of Geophysical Research*, *112*, L22107. https://doi.org/10.1029/2007JA012260

Turner, D. L., Shprits, Y., Hartinger, M., & Angelopoulos, V. (2012). Explaining sudden losses of outer radiation belt electrons during geomagnetic storms. *Nature Physics*, *8*, 208–212. https://doi.org/10.1038/nphys2185

Ukhorskiy, A. Y., Shprits, Y. Y., Anderson, B. J., Takahashi, K., & Thorne, R. M. (2010). Rapid scattering of radiation belt electrons by storm-time EMIC waves. *Geophysical Research Letters*, *37*, L09101. https://doi.org/10.1029/2010GL042906

Usanova, M. E., Drozdov, A., Orlova, K., Mann, I. R., Shprits, Y., Robertson, M. T., … Wygant, J. (2014). Effect of EMIC waves on relativistic and ultrarelativistic electron populations: Ground-based and Van Allen Probes observations. *Geophysical Research Letters*, *41*, 1375–1381. https://doi.org/10.1002/2013GL059024

Xiao, F., Su, Z., Zheng, H., & Wang, S. (2009). Modeling of outer radiation belt electrons by multidimensional diffusion process. *Journal of Geophysical Research*, *114*, A03201. https://doi.org/10.1029/2008JA013580

Xiao, F., Su, Z., Zheng, H., & Wang, S. (2010). Three-dimensional simulations of outer radiation belt electron dynamics including cross-diffusion terms. *Journal of Geophysical Research*, *115*, A05216. https://doi.org/10.1029/2009JA014541

Xiao, F., Yang, C., Su, Z., Zhou, Q., He, Z., He, Y., … Blake, J. B. (2015). Wave-driven butterfly distribution of Van Allen belt relativistic electrons. *Nature Communications*, *6*, 8590. https://doi.org/10.1038/ncomms9590